Hierarchical modelling of turbulence and geometry for fan flows

Wang, Zhong-Nan; Tucker, Paul G.

DOI:
10.2514/6.2021-2767

Document Version
Peer reviewed version

Citation for published version (Harvard):
Wang, Z-N & Tucker, PG 2021, Hierarchical modelling of turbulence and geometry for fan flows. in *AIAA Aviation 2021 Forum.*, AIAA2021-2767, American Institute of Aeronautics and Astronautics Inc. (AIAA), AIAA AVIATION 2021 Forum, 2/08/21. https://doi.org/10.2514/6.2021-2767

Hierarchical Turbulence and Geometry Modelling of Fan Flows

Zhong-Nan Wang[1] and Paul G. Tucker[2]
Department of Engineering, University of Cambridge, Cambridge, UK

Flow separations occur in the tip region when the fan is operating at the approach condition. To reduce computational cost without degrading accuracy, the hierarchical modelling approach has been developed to predict such fan flow. This allows both flow and geometry to be treated with various fidelity levels in different zones. To be specific, this is achieved by zonalising Large-Eddy Simulation (LES) in the fan tip region and modelling downstream stators with low-order blade body forces. This approach provides an accurate and economical prediction of separated fan flows in the stage environment. The predicted fan wake profiles show a fairly good agreement with the hot-wire measurements considering passage-to-passage variations.

Nomenclature

c	=	chord, *m*
ρ	=	density, kg/m^3
u_i	=	velocity in x_i direction, *m/s*
E	=	total internal energy, *J*
f	=	blending function for hybrid LES-RANS
H	=	total enthalpy, *J*
p	=	static pressure, *Pa*
q_i	=	heat conduction in x_i direction, J/m^2
$\dot{q}_v$	=	volumetric heat source, J/m^3
$f_{b,i}$	=	blade body force in x_i direction, N/m^3
λ	=	blade blockage factor
μ	=	viscosity, $Pa \cdot s$
ω	=	vorticity, s^{-1}
τ_{ij}	=	viscous stress tensor, N/m^2

I. Introduction

As the bypass ratio increases to pursue higher engine efficiencies, the fan becomes a key contributor to thrust and also noise. When an aircraft is landing, the fan is running at a lower speed, leading to excessive separation in the tip region. Even within the stable operation range, this separation will also lead to significant aerodynamic loss and noise emission. The noise is composed of tonal and broadband components. The tonal noise has been fairly well reduced by frequency-tuned acoustic liners, which makes the broadband component stand out. Broadband noise is closely related to the turbulence generated in the fan separations and wakes. This emphasises the importance of accurate prediction of fan turbulence. On the other hand, the engine is now made increasingly compact to reduce weight and aerodynamic drag. This results in stronger interaction between adjacent components. In the fan configuration, the fan blade is neighboured by a bypass splitter ring as well as bypass and core duct stators. The downstream effects are not negligible on the development of fan separation and wake. The complexity of both turbulence and geometry in this fan stage, sketched in Fig. 1, make the simulation of this closely coupled fluid system extremely challenging. This type of simulation has also been listed as one of the grand challenges in the NASA CFD Vision 2030 [1]. The challenge comes from two main aspects. First, the separation and wakes need to be predicted

[1] Lecturer, College of Engineering and Physical Sciences, University of Birmingham, Member AIAA
[2] Rank Professor of Engineering, Department of Engineering, University of Cambridge, Associate Fellow AIAA

by high-fidelity simulations, such as Direct Numerical Simulation (DNS) and Large-Eddy Simulation (LES), but they are prohibitively expensive to be used for the whole fan stage. Second, the modelling and meshing process of complex geometries is difficult and time-consuming, considered as the main barriers to CFD autonomy, especially for bypass fan configurations with stationary and rotating components. Even if the mesh could be automatically generated, the generation process for such large-scale high-fidelity simulations still faces other issues with the effective utilization of high-performance computing [2]. One feasible solution to these could be: treat flow and geometry by zones with various modelling fidelities according to the local accuracy requirement. It could provide an accurate prediction of sophisticated turbulent flow features at a minimal computational effort. This forms the aims of this research.

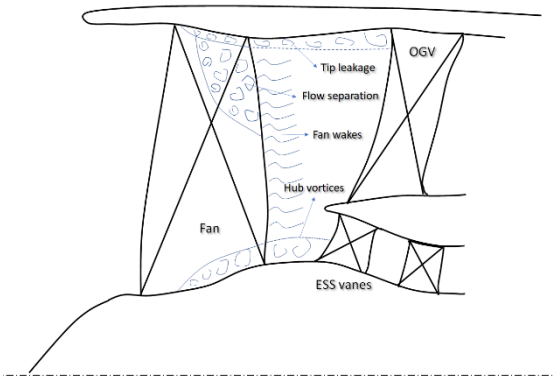

Fig. 1 Flow topology at the approach condition

Integrating different fidelity levels of turbulence and geometry modelling in one simulation allows an increase in computational speed. This enables the simulation of large-scale aerodynamically coupled systems at a minimum cost to meet the required accuracy. Conventionally, the degree of modelling in a simulation is described as the fidelity levels of a solution, and the fidelity decreases with modelled content. However, it is necessary to distinguish fidelity from accuracy. A low fidelity model, operating in the calibrated space, is able to reproduce results as well as a higher fidelity simulation. Rather, an increase in fidelity provides more flow detail and requires less empiricism. The coupled fluid problem can be solved by integrating models of different fidelities in one solution: flow zones with adequate knowledge solved by well-calibrated low-fidelity models while zones with little knowledge solved by high-fidelity eddy-resolving and fully geometry resolved methods. The consistent accuracy could be achieved in one solution with sufficient flow detail in the region of interest.

Turbulence and geometry modelling can be pursued in a coherent framework, as there is a hierarchy of methods from low to high fidelity levels with the structural similarities shared in the governing equations, shown in Fig. 2. With the increase of simulation fidelity, the modelled content decreases while the resolved content and simulation cost increase. For turbulence modelling, the hierarchy is built on how much of the turbulent scales are modelled. At the low fidelity end, Reynolds Averaged Navier-Stokes (RANS) equations are solved to model all turbulent scales, while at the high-fidelity end, the Navier-stokes equations are directly solved in DNS to resolve all the scales without modelling. LES trades off between the ends, resolving only the large-scale turbulent motion with grid cut-off scales modelled. A similar hierarchy exists in geometry modelling, which is less recognised than that of turbulence. This geometry modelling hierarchy depends on how much the geometry is explicitly resolved. The most common way is to resolve the full geometry using body-conformal mesh, which is at the top fidelity level. As mentioned before, this can be challenging for complex geometries and moving bodies. Going down the hierarchy, a body force is introduced to model the geometry instead of resolving on grids. Immersed Boundary Methods (IBM) were developed to represent the geometry on the Cartesian mesh using the distribution of body forces [3]. This has greatly offloaded the mesh generation task with a wide use for fluid-structure interactions. For the internal turbomachinery flows, the IBM could be simplified by filtering out the blade geometry with azimuthal homogenous distributed blade forcing terms [4]. This is referred to as IBMfg – IBM with filtered geometry (fg) - in this paper. As only the radial profile of azimuthally-averaged flow is captured in IBMfg, it is placed at the low-fidelity end. For both geometry and turbulence modelling, the hybridization could be made across the hierarchy to zonalise the high-fidelity method in the region where it is needed most. Several attempts have been successful from either turbulence or geometry modelling aspects. Typical examples for hybrid turbulence modelling are Detached Eddy Simulation (DES) [5], Zonal DES (ZDES) [6] and Embedded LES [7], while the hierarchical geometry modelling can also be found in a few cases [8-10].

In this research, an attempt has been made by combining hierarchical modelling of both geometry and turbulence in one simulation for fan stage flows. This is achieved by zonalising LES in the fan tip region for separated flows and

lower-order modelling the downstream stators with IBMfg. The paper is organized as follows: First, the governing equations are introduced for the hierarchical modelling of geometry and turbulence. The implementation of the hierarchical modelling strategy is then given for the fan stage. Finally, the hierarchical method is validated by comparing the prediction with experimental measurements and the effects of the RANS-LES interface are briefly discussed.

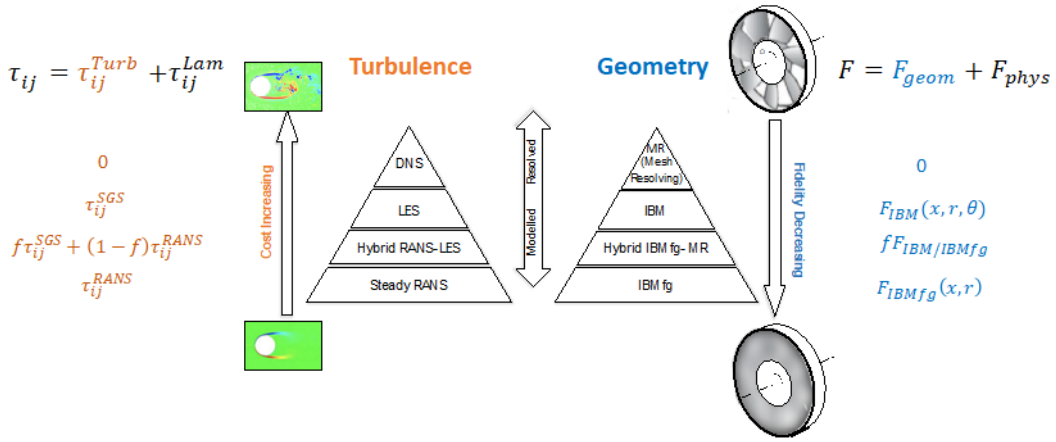

Fig. 2 Hierarchy of turbulence and geometry modelling, adapted from Ref. [11]

II. Methodology

A. Governing equations of hierarchical turbulence and geometry modelling

The structural similarities in the governing equations provide the theoretical foundation for a hierarchy of turbulence and geometry models. The governing equations are given in a general integral form, discretised by finite volume method:

$$\frac{\partial}{\partial t}\int_{\Omega} \boldsymbol{Q}dV + \oint_{\Gamma} \boldsymbol{G_i} n_i \, dA = \int_{\Omega} \boldsymbol{F}dV \tag{1}$$

where $\boldsymbol{\Omega}$ and $\boldsymbol{\Gamma}$ are control volume and surfaces of a mesh cell in the computational domain, and n_i is the x_i component of a unit surface normal vector pointing outwards. $\boldsymbol{F}$ represents volumetric source/force, which contains both physical sources $\boldsymbol{F_{phys}}$ and geometry forcing $\boldsymbol{F_{geom}}$. The physical sources $\boldsymbol{F_{phys}}$ refers to the volumetric sources induced by any physical processes, such as volumetric heat, buoyance, gravity, Coriolis and centrifugal forces. The geometry force refers to the force exerted on fluid particles from the geometry boundaries and will be discussed later in detail. The conservative variables $\boldsymbol{Q}$, convective and viscous flux $\boldsymbol{G_i}$ are written as

$$\boldsymbol{Q} = \begin{bmatrix} \rho \\ \rho u_1 \\ \rho u_2 \\ \rho u_3 \\ \rho E \end{bmatrix}, \boldsymbol{G_i} = \begin{bmatrix} \rho u_i \\ \rho u_1 u_i + p\delta_{i1} - \tau_{i1} \\ \rho u_2 u_i + p\delta_{i2} - \tau_{i2} \\ \rho u_3 u_i + p\delta_{i3} - \tau_{i3} \\ \rho H u_i - \tau_{ij} u_j + q_i \end{bmatrix} \tag{2}$$

The definition of viscous stress tensor τ_{ij} and source term $\boldsymbol{F}$ leads to a hierarchy of turbulence and geometry models.

For turbulence modelling, there are similarities shared by the RANS, LES and DNS equations. Although the primitive variables solved in the equations are ensemble-averaged in RANS and spatially filtered in LES, the key difference lies at the modelled turbulent stress tensor τ_{ij}^{turb} within the total viscous stress tensor

$$\tau_{ij} = \tau_{ij}^{lam} + \tau_{ij}^{turb} \tag{3}$$

where τ_{ij}^{lam} is the physical/laminar viscous tensor. In DNS, the modelled turbulent stress τ_{ij}^{turb} is zero as all the turbulent scales are directly resolved on grids. This modelled term appears in LES and RANS, and can be framed in a general form:

$$\tau_{ij}^{turb} = (1-f)\tau_{ij}^{RANS} + f\tau_{ij}^{LES} \tag{4}$$

where τ_{ij}^{RANS} is the Reynolds stress tensor provided by RANS modelling and τ_{ij}^{LES} is the subgrid stress tensor modelled in LES to account for unresolved turbulence scales. If f is a global parameter, the simulation will be run in pure LES ($f = 1$) or pure RANS ($f = 0$) mode. If $f(\boldsymbol{x})$ is a spatial blending function between 0 and 1, it defines the strategies of hybrid LES-RANS. This stress blending formulation (4) is able to incorporate the concept of wall-modelled LES, zonal/embedded LES and DES-type of methods. It is also worth noting that the τ_{ij}^{RANS} and τ_{ij}^{LES} can be provided

independently using different RANS models and LES subgrid models. In the current simulation, the LES stress is provided by Wall-Adapting Local Eddy-Viscosity (WALE) subgrid model [12] and the RANS stress is provided by the one-equation Spalart-Allmaras model [13].

For geometry modelling, the hierarchy is reflected in the definition of geometry forcing $\boldsymbol{F_{geom}}$, as shown in Fig. 2. When $\boldsymbol{F_{geom}} = \mathbf{0}$, the simulation is performed with direct mesh-resolved geometries. In the IBM, non-zero localised $\boldsymbol{F_{geom}}$ is introduced to model the force exerted on fluids by solid boundaries instead of resolving the real geometry by body-conformal mesh. The fidelity level in the IBM category depends on how accurate F_{geom} describes the geometry. In the normal IBM, $\boldsymbol{F_{geom}}$ is a function of three-dimensional coordinates $\boldsymbol{x} = (x, r, \theta)$ that exactly enforces the effect of discrete real geometry boundaries. Moving to lower fidelity levels, more geometry features become filtered and will be modelled. In the IBMfg, which is used in this research, the blade/stator geometry is circumferentially filtered out with its azimuthal mean effect modelled by the two-dimensional body force

$$\boldsymbol{F_{geom}}(x,r) = \begin{bmatrix} 0 \\ f_{b,1} + \frac{1}{\lambda} p \frac{\partial \lambda}{\partial x_1} \\ f_{b,2} + \frac{1}{\lambda} p \frac{\partial \lambda}{\partial x_2} \\ f_{b,3} + \frac{1}{\lambda} p \frac{\partial \lambda}{\partial x_3} \\ f_{b,i} u_i \end{bmatrix} \tag{5}$$

where $f_{b,i}$ is the blade force acting on the fluid in the direction x_i, and λ is the factor that accounts for the blade thickness blockage. The body force term $f_{b,i}$ and blockage factor λ are only active in the blade/stator region.

The blade forcing term $f_{b,i}$ consists of two parts

$$f_{b,i} = f_{bn,i} + f_{bp,i} \tag{6}$$

where $f_{bn,i}$ is the normal blade force that enforces non-permeable boundary and guides the flow turning along the blade camber line. This is implemented using the proportional integral (PI) controller which drives the computed velocity u_i^n to the desired velocity u_i^D at the smeared blade region.

$$f_{bn,i} = K_p(u_i^D - u_i^n) + K_I \int_0^{t_n} (u_i^D - u_i^n) dt \tag{7}$$

In the above, K_p is the coefficient of proportional controllers with dimension of s^{-1} and controls the convergence speed to the desired value as a damping factor. K_I is the coefficient of the integral controller with dimension s^{-2} and is used to increase computational stability. $f_{bn,i}$ will vanish when the computed velocity is parallel to the blade camber line. $f_{bp,i}$ is the parallel blade force that is calibrated to model the blade profile and endwall loss. This IBMfg has been well validated and was used to study the mutual interactions between intake-distortion and fan in our previous research [14, 15].

B. Hierarchical modelling strategy for fan stage flows

Fig. 3 shows the simulation strategy of a fan stage with bypass duct configuration. The fan is running at half of the design speed, the mismatch between flow and blade angle causes excessive separation in the tip region. Hence, the LES is zonalised in the fan tip to capture complex tip flows, including separation on the blade and endwall as well as leakage from the tip gap. Compared to the tip flows, the flow in the lower span is relatively clean without too much separation. Hence, RANS is used in this region to save computational cost. The interface between RANS and LES is placed at approximately 50% span in the fan region and follows a streamline in the meridional plane. As our research is focused on the fan flow, the downstream stators, including OGV in the bypass and ESS in the core, are modelled in a low-order way using IBMfg, which predicts the azimuthally averaged behaviour of the stators. This provides the fan with a suitable outlet condition from downstream stators but without substantial increase of computational cost.

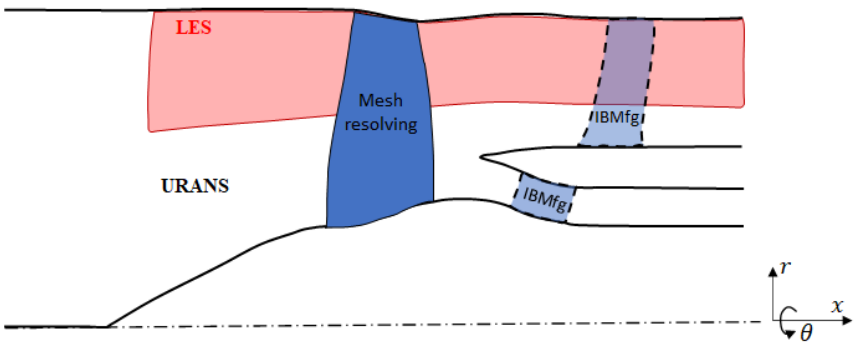

Fig. 3 Schematics of hierarchical modelling strategy of a fan stage

Fig. 4 shows the implementation of hybrid LES-RANS modelling based on the turbulence stress blending function f that is given in Eq. (4). The function f is set to one to zonalise LES in the fan tip region from the 50% span location. The rest of the region is left with $f = 0$ in the RANS mode. In the LES zone, a thin RANS layer of $y^+ \sim 100$ is placed near the fan blade and casing as a wall model. This avoids the cost of resolving near-wall turbulent streaks. The hierarchical modelling strategy was implemented in an unstructured edge-based solver for compressible flows. The kinetic energy preserving scheme [16] is used to keep the numeric at a low dissipation level that is suitable for LES. The time advancement is achieved using the 2nd order backward Euler difference with dual time stepping. The simulation is performed in the rotational framework with absolute boundary conditions set at the inlet and outlets. The total temperature and pressure are imposed at the inlet and static pressure with radial equilibrium conditions are set at both bypass and core duct outlets.

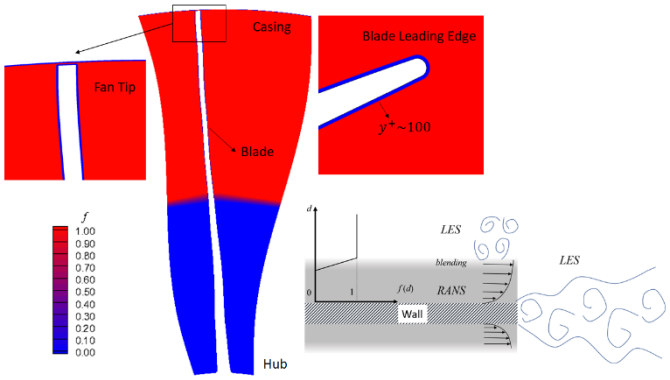

Fig. 4 Blending function distribution of zonalised LES in the fan passage

Hexahedral mesh cells are used here to improve mesh quality although the flow solver was written for computation on unstructured meshes. The fan blade is mesh-resolved while downstream stators are modelled by IBMfg without geometry conformal mesh blocks. The mesh around the fan blade is illustrated in Fig. 5. An O-grid is employed to provide high-quality orthogonal mesh to the boundary layers on blade and endwall surfaces. The grid spacings are listed in Table 1. Grid points are clustered around blade leading and trailing edges and gradually expanded into the mid-chord with maximum streamwise grid size $\Delta s^+ = 600$ in terms of wall units. The first cell wall distance Δd_w^+ on the blade and endwalls are between 0.5 and 3. The maximum spanwise grid size Δr^+ in LES zone is around 300. These all satisfy the grid density requirement of hybrid RANS-LES [17]. This leads to a total of 63 million cells, while the mesh count is 3-6 billion for the wall resolving LES of a whole-span fan.

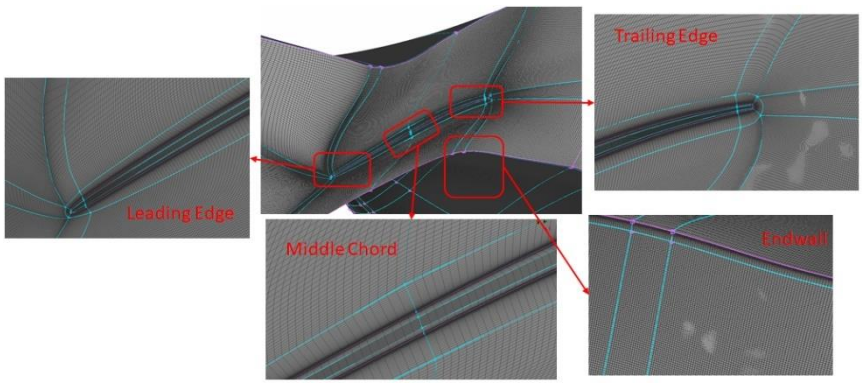

Fig. 5 Mesh distribution in the fan region

Table 1 Streamwise grid size distribution along fan blade surface

Locations	Leading Edge	20% c	50% c	80% c	Trailing Edge
Δs^+	10	100	600	150	15

III. Results and Discussions

A. Instantaneous flow field

Zonalised LES has been performed in the upper span of the fan passage. Fig. 6 shows the flow structures from this simulation. The flow structures are visualised by Q-criterion isosurfaces. Fine-scale turbulence has been well resolved by LES from the fan tip to the middle span while ensemble-averaged large-scale wake structures and horse-shoe hub vortices are captured by RANS. A close-up view of the tip region shows the structures resolved by LES. The hairpin vortices roll up near the leading edge and flow separations occur on the fan blade in the upper span. This is due to the positive flow incidence at this off-design rotational speed which is half of the design speed. In the tip region, the incoming boundary layer at the casing stagnated around the fan blade leading edge and generates horse-shoe vortices in the tip corner. The tip leakage flows are weak compared to the horseshoe vortices because the small tip clearance is relatively small, which is 0.28 percent of span length.

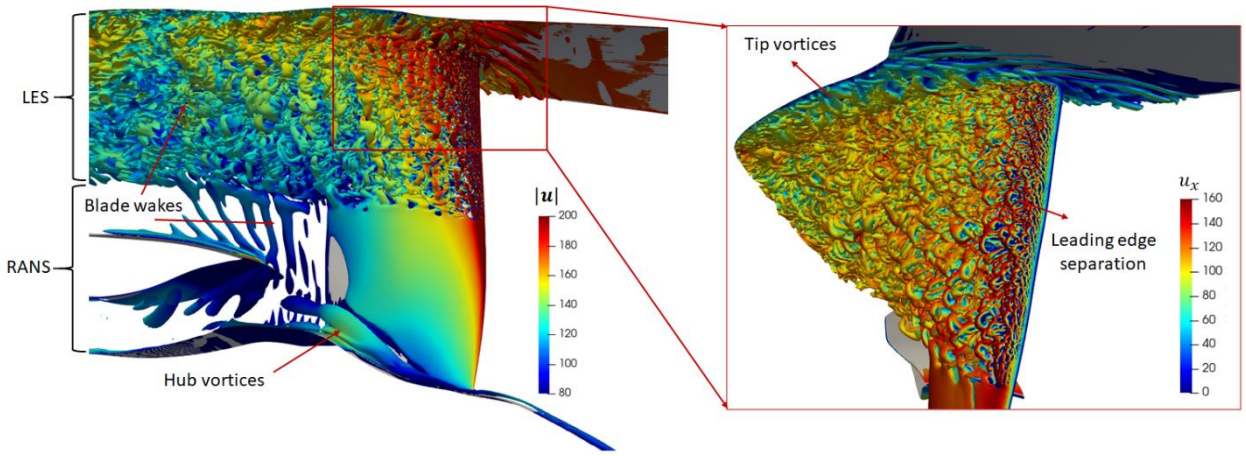

Fig. 6 Q-criterion isosurfaces illustrated flow structures by zonalised LES in the fan tip region

Fig. 7 shows the ratio of turbulence modelling and physical/laminar viscosity and the vorticity magnitude at an axial plane located around 33 percent fan chord c downstream of the fan. The majority of turbulent energy is directly resolved on grids by LES rather than modelled by the viscosity. This is opposite in RANS, where most of the turbulent energy is modelled. Hence, the turbulence modelling viscosity is high in the wake of the lower-span RANS region and fades away towards the fan tip in the upper-span LES region. This modelling difference is also reflected in the vorticity. LES is zonalised in the upper span, resolving fine-scale turbulent structures in the wake and endwall regions.

The flow field makes a smooth transition into the reduced flow-scale RANS region in the lower span. This indicates that the LES has been successfully blended into the RANS context.

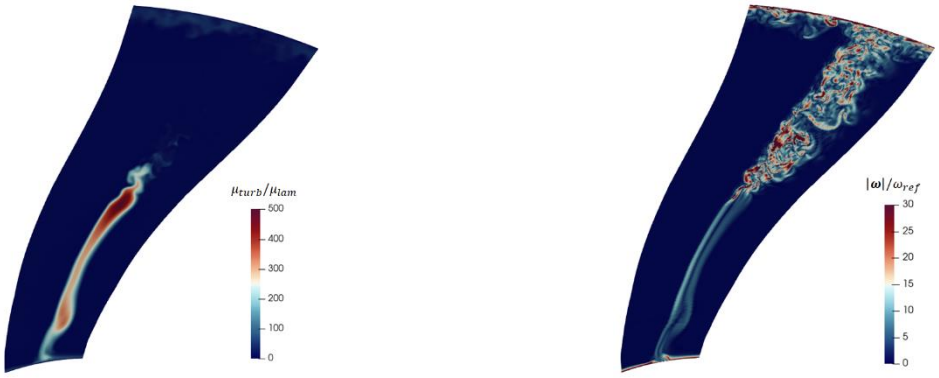

(a) the ratio of turbulent eddy viscosity to physical viscosity (b) vorticity magnitude

Fig. 7 RANS eddy viscosity and vorticity magnitude in the hot-wire measurement plane downstream of the fan blade

B. Time-averaged flow fields

The time-averaged flow fields from the simulation are compared with the experimental measurement at the same plane downstream of the fan. The experimental measurements were performed using hot wires at a interstage position with a fixed azimuthal location and 33 radial transverse positions [18]. The averaged flow fields from experimental measurements are obtained by phase averaging. Fig. 8 shows the comparison of axial velocity between simulation and experiment. Passage-to-passage variations are present in the experiment. This could be caused by the manufacture and installation variation of the fan blades as well as the mechanical vibration during the operation. In the simulation, only one blade passage is computed and repeated 20 times to form the whole annulus. The same contour levels are used for this comparison. The LES captures the fan suction surface separation and the wake shape shows a qualitative agreement with that of the experiment in the upper span. RANS is smoothly blended with LES and yields a reasonable prediction of the low-span flow.

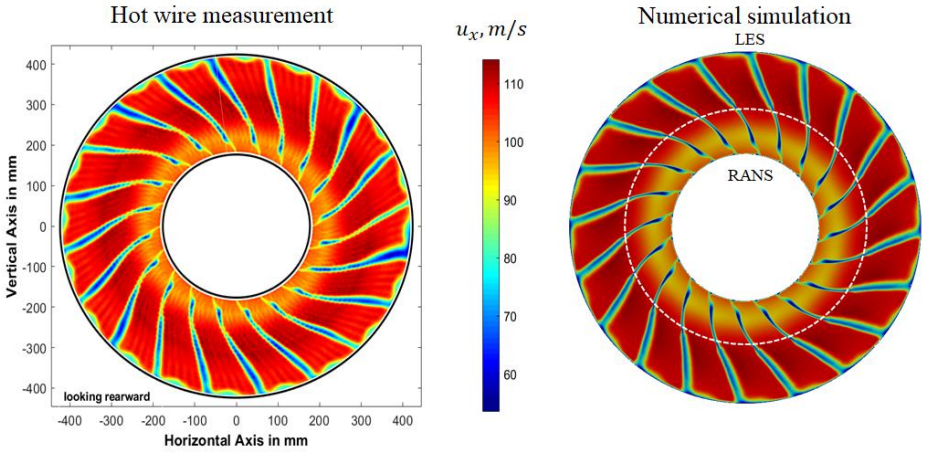

Fig. 8 Axial velocity from hot-wire measurements and numerical simulation downstream of the rotor

Fig. 9 compares the turbulent fluctuations of axial velocity from both experiment and simulation. In the simulation, the turbulent fluctuations are hardly seen in the lower span, because they are intrinsically modelled in RANS instead of resolved on grids in LES that is used in the upper span. The comparison between simulation and measurement on the turbulent fluctuations are therefore focused at the upper span. Although the experiments show large passage-to-passage variations, the LES generally captures the shape of high fluctuations regions. The predicted fluctuation level is in a reasonable range compared to that of experiment. In the tip, the high fluctuation and low-velocity region is caused by tip leakage flows and casing horseshoe vortices. This is slightly under-predicted by the simulation. A possible reason is that the tip clearance is larger in the experiment than the designed value used in the simulation. Overall, a qualitative agreement has been achieved between simulation and experiment.

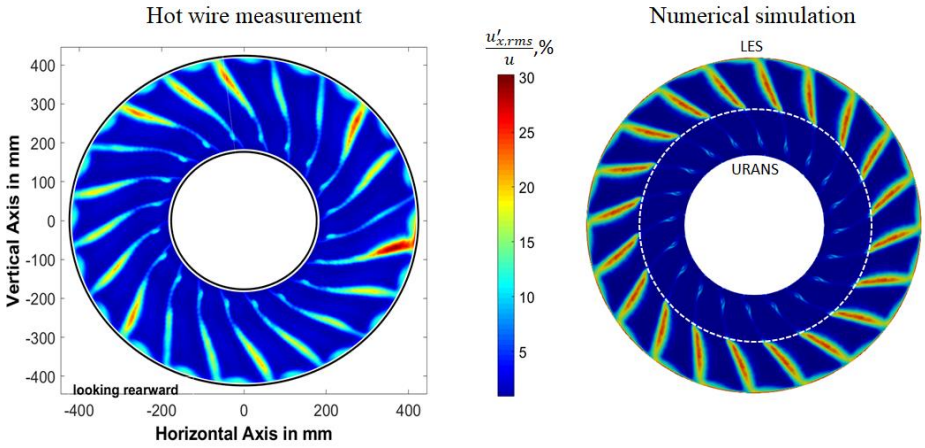

Fig. 9 Turbulent fluctuations of axial velocity downstream of the rotor

C. Wake profiles

The wake profiles are quantitively compared with the experimental measurements at various radial locations. Fig. 10 shows the azimuthal velocity profiles across the wake in the upper-span LES region. Four radial locations, *i.e.* 90%, 80%, 70% and 60% of the span, are selected for this comparison. The measured wake profile from a reference passage is plotted as a solid line. The variations across passages are represented in shaded areas. The LES prediction of axial velocities, plotted by red circles, shows an excellent agreement with the reference passage measurement in terms of the wake depth and width. The blade wake reaches a maximum width near 70% span because of the separation on the suction surface. LES predictions of radial and tangential velocities also show a reasonable agreement with the measurements, although consistent overprediction is observed. This overprediction is also present in the eddy-resolving predictions of the other partners in the same EU project using wall modelled LES [19] and ZDES [20]. This indicates a possibility of hot-wire measurement uncertainty. However, the overall shape and location of the wake is well captured and most of the predictions lie close to the range of passage-to-passage variation.

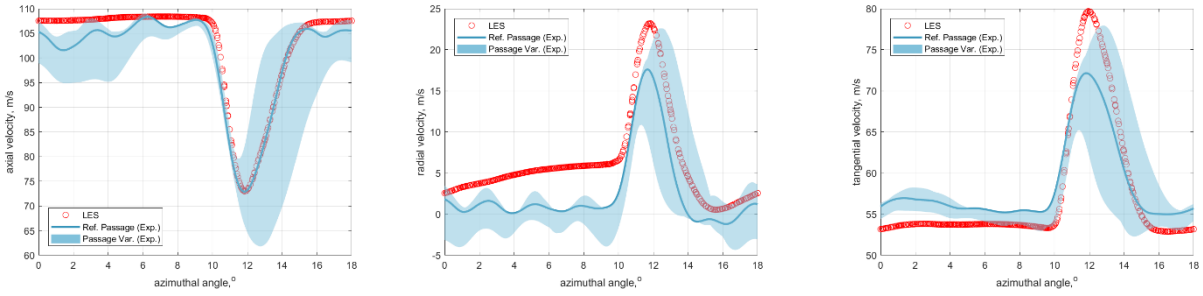

(a) 90% span

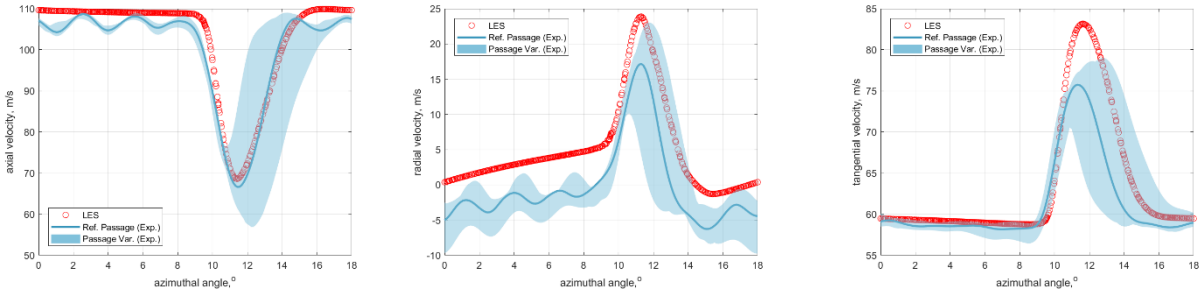

(b) 80% span

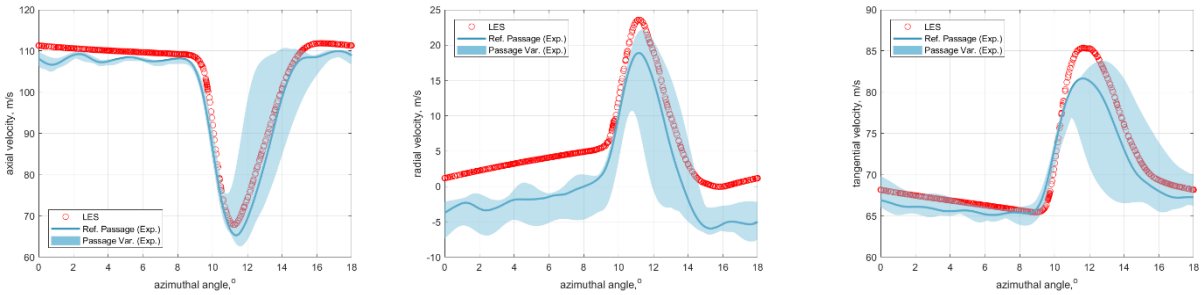

(c) 70% span

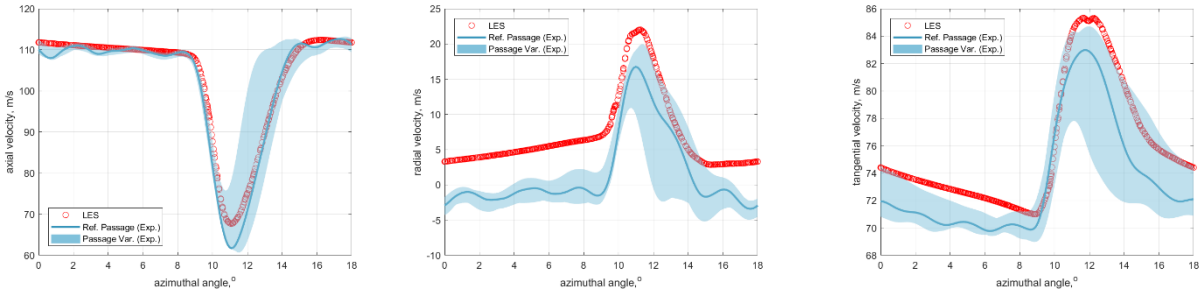

(d) 60% span

Fig. 10 Azimuthal velocity wake profiles at the 90%, 80%, 70% and 60% span locations in the interstage measurement plane downstream of the fan rotor

The azimuthal variation of velocity fluctuations is shown in Fig. 10. These are at the same span locations as the velocity profiles. The LES generally agrees with the measurements and lies within the passage variations. There are two peaks in the profiles at the 90% span. The first peak is caused by the tip vortices. This is slightly underpredicted by LES as the tip clearance in the simulation might be different from that in the experiment. The first peak disappears at lower span locations while the second peak remains. The second peak, corresponding to the blade wake, is reasonably predicted by LES. Within the passage-to-passage variation, the prediction is generally higher than that in the reference passage. This could be related to the frequency cut-off in the measurement because of the wire size. This potentially leads to a low measured turbulent intensity [21] and this overprediction is also consistent with that of the wall modelled LES [19] and ZDES [20] of our project partners. The overall agreement between simulation and experiment is satisfactory taking all these factors into account.

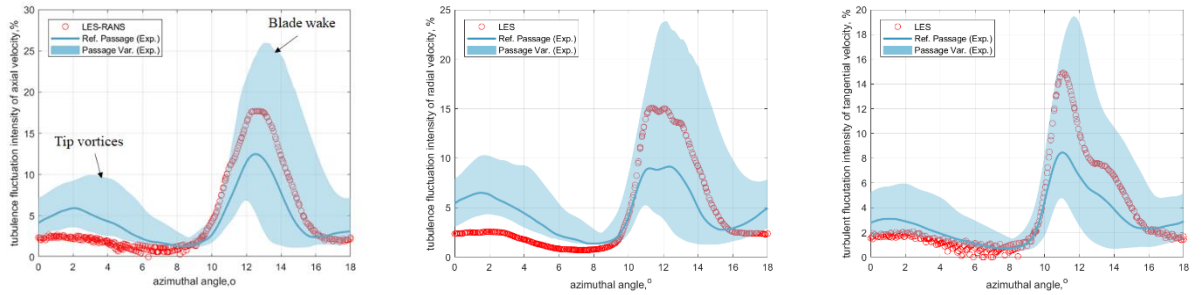

(a) 90% span

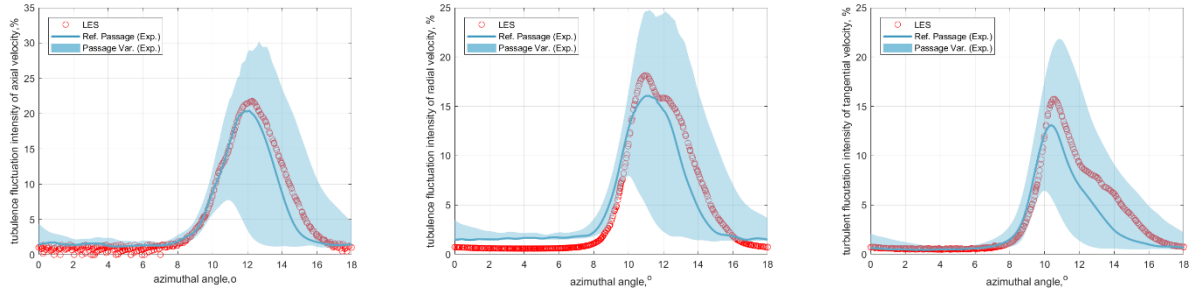

(c) 80% span

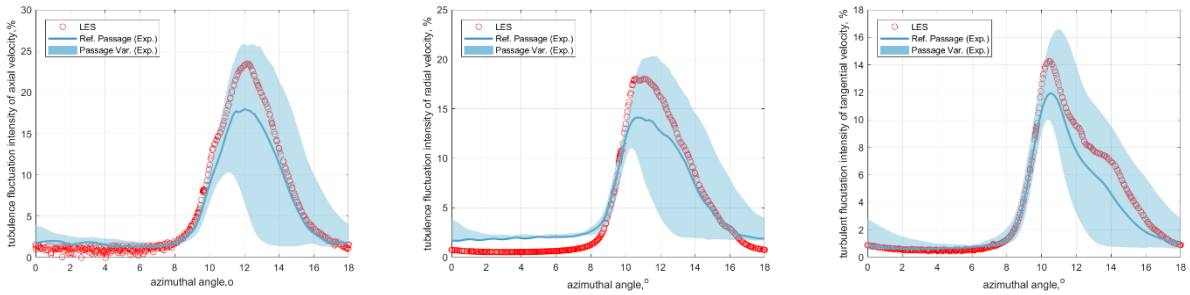

(d) 70% span

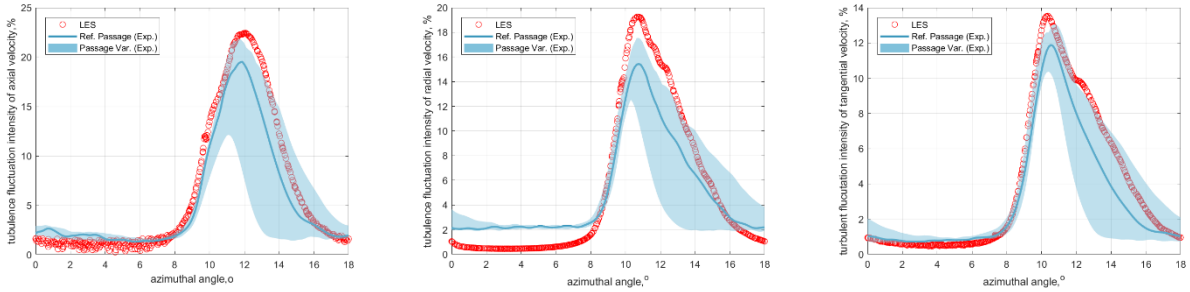

(e) 60% span

Fig. 11 Azimuthal wake profiles of velocity fluctuations at the 90%, 80%, 70% and 60% span locations in the interstage measurement plane downstream of the fan rotor

In the lower-span RANS region, the axial velocity profiles are plotted against the measurements in Fig. 12. Since the one equation SA model is used for RANS modelling, the axial velocity turbulent fluctuation is not directly available to compare with the measurements. However, the wake velocity profiles are reasonably predicted by RANS when compared with the measurements. The wake shape and location are well captured, but with a thinner and deeper wake predicted. This is a well-known deficit of RANS models. The results indicate that RANS has been successfully integrated with LES and is able to generate reasonably accurate results in a less separated flow region.

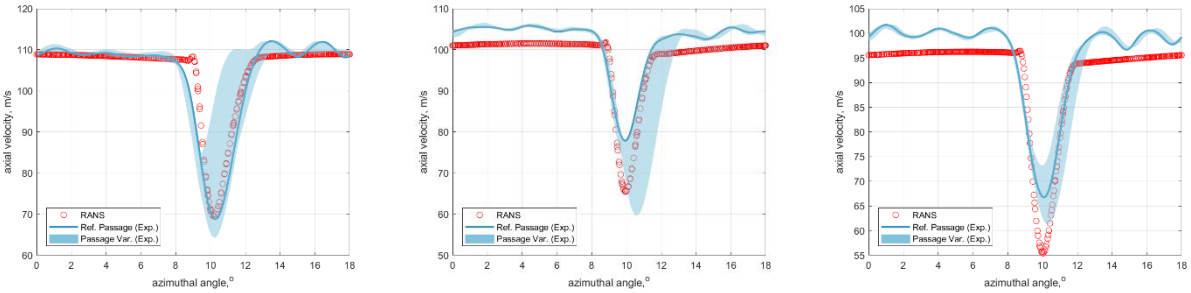

(a) 40% span (b) 30% span (c) 20% span

Fig. 12 Azimuthal profile of axial velocity at 40%, 30% and 20% span locations in the interstage measurement plane downstream of the fan rotor

D. Effects of RANS-LES interface

In the current simulation, the RANS-LES interface has been placed at 50% span following a streamline. It is worth assessing if the interface will affect the current results. To investigate sensitivity of RANS-LES interface position, the interface is moved from the 50% to 40% span. The axial velocity and its fluctuations are plotted in Fig. 13 directly at the two interfaces, *i.e.* 50% and 40% span, and compared with the measurements to evaluate interface effects. At the 50% span location, the interface shows negligible effects on the velocity prediction, as the axial velocity is well predicted by the simulation with the LES-RANS interface at the same span location. The turbulent fluctuations are slightly overpredicted in the wake, but the shape and location have been captured. Consistency is observed between the two simulations with different interface locations, suggesting little sensitivity of interface locations. This is also verified by the results at the 40% span location. Fig. 13(b) shows that the predicted velocity profiles of the two

simulations align close to each other and agree fairly well with the reference passage and within the passage-to-passage variation. The turbulent fluctuations are also reasonably predicted by the simulation with 40% span interface. For the simulation with 50% span interface, the 40% span location is in the RANS region where the turbulent fluctuations are not resolved, hence the predicted turbulent fluctuations are at a low level. To further check if the interface will affect LES and RANS regions, the wake profiles at two span locations are plotted in Fig. 14. The two span locations, *i.e.* 60% and 30%, are relatively close to the interfaces and located in the LES and RANS regions respectively. Good agreement is obtained between the two simulations with different LES-RANS interfaces. Overall, the LES-RANS interface and its position is shown to have no significant effects on the simulation results and the proposed turbulence modelling strategy is robust.

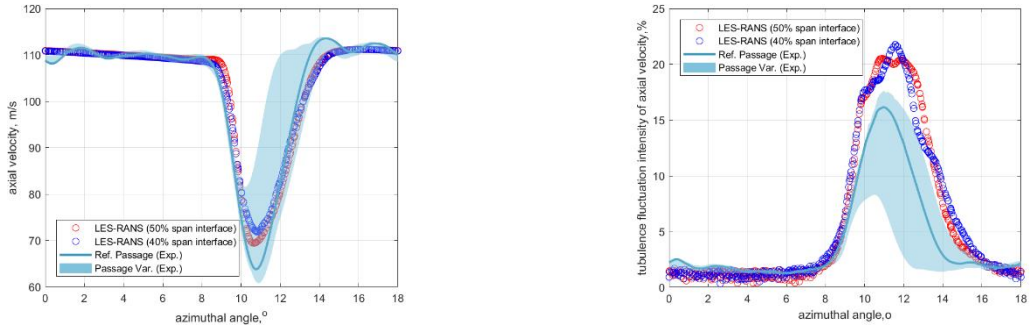

(a) 50% span

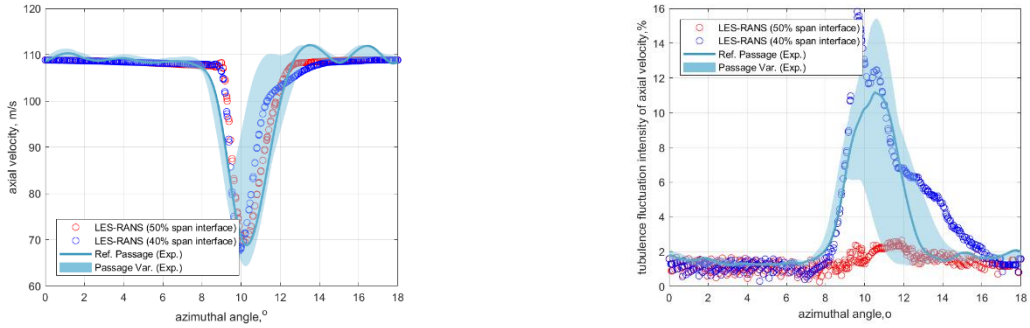

(b) 40% span

Fig. 13 Azimuthal profiles of axial velocity and its fluctuations at the RANS-LES interfaces of the two simulations, *i.e.* 50% and 40% span

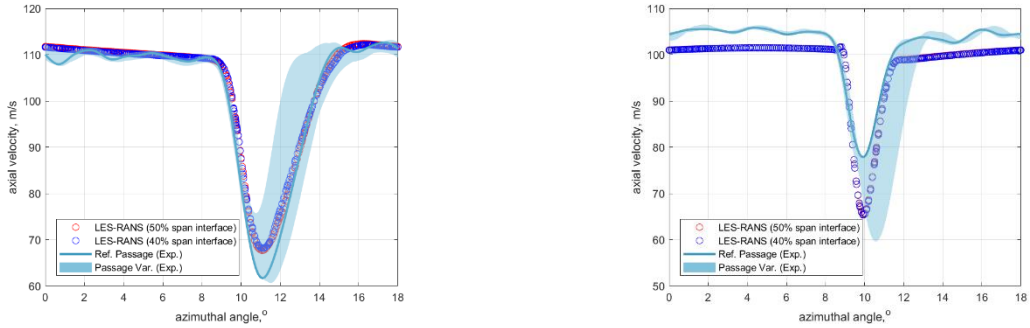

(a) 60% span (LES region) (b) 30% span (RANS region)

Fig. 14 Comparison of azimuthal profiles of axial velocity and its fluctuations of the two simulations at the 60% and 30% span, representing the results in the LES and RANS regions respectively

IV. Conclusion

Challenges are faced to simulate coupled fluid systems with complex geometry and turbulence. A modelling hierarchy of turbulence and geometry is explored in this paper to reduce the computational effort. In the developed hierarchical modelling approach, the flow and geometry can be simulated zonally at various fidelity levels. This method has been successfully applied to a fan stage with bypass configuration. The fan operated at half of the design speed, leading to excessive separation in the tip region. For turbulence modelling, LES is zonalised in the upper half span to predict the separated flow and the tip leakage, while RANS is used to simulate the relatively clean hub flow. For geometry modelling, the fan blade is resolved by grids while the downstream stators are modelled using IBMfg, where the stator geometry is filtered by imposing azimuthally homogeneous body forces. The simulation is performed with 63 million cells compared with 3-6 billion cells in a proper wall-resolved LES. In the simulation, fine-scale turbulence is well resolved in the LES zone and a smooth transition is achieved into the RANS region where ensemble-averaged large-scale flow motions are recovered. The simulation has been systematically compared with hot wire measurements at the interstage. Overall, high accuracy is achieved by this hierarchical modelling. In the upper half span, the LES prediction is compared with the measurements in terms of the mean velocities and the turbulent fluctuations. The LES prediction shows a satisfactory agreement with the measurements in the reference passage and within the passage-to-passage variation. In the lower half span, wake profiles are also predicted by RANS with expected accuracy. The interface of RANS and LES is shown with minimal effects on the overall flow prediction. In the future, the fan wake data will be used to provide an assessment of fan wake modelling assumption and explore the underlying mechanisms of fan tip noise generation.

Acknowledgements

The work is funded in the EU H2020 project “TurboNoiseBB” under grant agreement No. 690714. The computational time was provided by the UK turbulence consortium under the EPSRC grant EP/L000261/1 on UK national supercomputer ARCHER and also by the EPSRC RAP project on Tier-2 machine CSD3 at Cambridge.

References

[1] Slotnick, J., Khodadoust, A., Alonso, J., Darmofal, D., Gropp, W., Lurie, E., and Mavriplis, D., 2014, "CFD vision 2030 study: a path to revolutionary computational aerosciences," National Aeronautics and Space Administration, Langley Research Center, pp. NASA/CR-2014-218178.

[2] Chawner, J. R., and Taylor, N. J., "Progress in Geometry Modeling and Mesh Generation Toward the CFD Vision 2030," AIAA Aviation 2019 Forum.

[3] Mittal, R., and Iaccarino, G., 2005, "Immersed boundary methotds," Annual Review of Fluid Mechanics, 37(1), pp. 239-261.

[4] Cao, T., Hield, P., and Tucker, P. G., 2017, "Hierarchical immersed boundary method with smeared geometry," Journal of Propulsion and Power, pp. 1-13.

[5] Spalart, P. R., 2009, "Detached-eddy simulation," Annual Review of Fluid Mechanics, 41, pp. 181-202.

[6] Deck, S., 2012, "Recent improvements in the Zonal Detached Eddy Simulation (ZDES) formulation," Theoretical and Computational Fluid Dynamics, 26(6), pp. 523-550.

[7] Holgate, J., Skillen, A., Craft, T., and Revell, A., 2019, "A Review of Embedded Large Eddy Simulation for Internal Flows," Archives of Computational Methods in Engineering, 26(4), pp. 865-882.

[8] Ma, Y., Cui, J., Vadlamani, N. R., and Tucker, P., 2019, "Hierarchical geometry modelling using the immersed boundary method," Computer Methods in Applied Mechanics and Engineering, 355, pp. 323-348.

[9] Ma, Y., Cui, J., Vadlamani, N. R., and Tucker, P., 2018, "Effect of Fan on Inlet Distortion: Mixed-Fidelity Approach," AIAA journal, 56(6), pp. 2350-2360.

[10] Ubald, B. N., Watson, R., Cui, J., Tucker, P., and Shahpar, S., 2021, "Application of an Immersed Boundary Method on an Instrumented Turbine Blade With Large Eddy Simulation," Journal of Turbomachinery, 143(11).

[11] Tucker, P. G., and Wang, Z. N., 2020, "Eddy Resolving Strategies in Turbomachinery and Peripheral Components," Journal of Turbomachinery, 143(1).

[12] Nicoud, F., and Ducros, F., 1999, "Subgrid-scale stress modelling based on the square of the velocity gradient tensor," Flow, Turbulence and Combustion, 62(3), pp. 183-200.

[13] Spalart, P. R., and Allmaras, S. R., 1994, "A one-equation turbulence model for aerodynamic flows," Recherche Aerospatiale, 1, pp. 5-21.

[14] Cao, T., Vadlamani, N. R., Tucker, P. G., Smith, A. R., Slaby, M., and Sheaf, C. T. J., 2016, "Fan–Intake Interaction Under High Incidence," Journal of Engineering for Gas Turbines and Power, 139(4).

[15] Cui, J., Watson, R., Ma, Y., and Tucker, P., 2019, "Low Order Modeling for Fan and Outlet Guide Vanes in Aero-Engines," Journal of Turbomachinery, 141(3).

[16] Jameson, A., 2008, "Formulation of kinetic energy preserving conservative schemes for gas dynamics and direct numerical simulation of one-dimensional viscous compressible flow in a shock tube using entropy and kinetic energy preserving schemes," Journal of Scientific Computing, 34(2), pp. 188-208.
[17] Tucker, P. G., 2016, Advanced computational fluid and aerodynamics, Cambridge University Press.
[18] Meyer, R., Hakansson, S., Hage, W., and Enghardt, L., "Instantaneous flow field measurements in the interstage section between a fan and the outlet guiding vanes at different axial positions," Proc. the 13th European Conference on Turbomachinery Fluid Dynamics and Thermodynamics.
[19] Lewis, D., Moreau, S., and Jacob, M. C., "Broadband Noise Predictions on the ACAT1 Fan Stage Using Large Eddy Simulations and Analytical Models," AIAA AVIATION 2020 FORUM.
[20] François, B., Barrier, R., and Polacsek, C., "Zonal Detached Eddy Simulation of the Fan-OGV Stage of a Modern Turbofan Engine," Proc. ASME Turbo Expo 2020: Turbomachinery Technical Conference and ExpositionV02AT32A004.
[21] Polacsek, C., Daroukh, M., Franc¸ois, B., and Barrier, R., "Turbofan Broadband Noise Predictions Based on a ZDES Calculation of a Fan-OGV Stage," Proc. Forum Acusticum.